Dynamic Hyporheic Zones

Singh, Tanu; Wu, Liwen; Gomez-Velez, Jesus D.; Lewandowski, Jörg; Hannah, David M.; Krause, Stefan

DOI:
10.1029/2018WR022993

Water Resources Research

RESEARCH ARTICLE
10.1029/2018WR022993

Dynamic Hyporheic Zones: Exploring the Role of Peak Flow Events on Bedform-Induced Hyporheic Exchange

Tanu Singh[1], Liwen Wu[2,3], Jesus D. Gomez-Velez[4], Jörg Lewandowski[2,3], David M. Hannah[1], and Stefan Krause[1]

[1]School of Geography, Earth and Environmental Sciences, University of Birmingham, Birmingham, UK, [2]Department of Ecohydrology, Leibniz Institute of Freshwater Ecology and Inland Fisheries, Berlin, Germany, [3]Geography Department, Humboldt-University, Berlin, Germany, [4]Department of Civil and Environmental Engineering, Vanderbilt University, Nashville, TN, USA

Key Points:
- A reduced-order model is used to systematically explore the dynamics of hyporheic zones during single peak flow events
- Exchange fluxes and residence times varied substantially with various combinations of peak flow characteristics, channel gradient, and streambed topography
- Even though the potential denitrification efficiency increased with high intensity and duration of the peak flow event, the extent of increase was determined by the interplay between geomorphological, biological, and hydrological controls

Correspondence to:
T. Singh,
t.singh.2@bham.ac.uk

Citation:
Singh, T., Wu, L., Gomez-Velez, J. D., Lewandowski, J., Hannah, D. M., & Krause, S. (2019). Dynamic hyporheic zones: Exploring the role of peak flow events on bedform-induced hyporheic exchange. *Water Resources Research*, *55*. https://doi.org/10.1029/2018WR022993

Received 21 MAR 2018
Accepted 6 DEC 2018
Accepted article online 14 DEC 2018

Abstract Discharge varies in space and time, driving hyporheic exchange processes in river corridors that affect biogeochemical cycling and ultimately control the dynamics of biogeochemical hot spots and hot moments. Herein, we use a reduced-order model to conduct the systematic analysis of the interplay between discharge variability (peak flow intensities, duration, and skewness) and streambed topography (bedform aspect ratios and channel slopes) and their role in the flow and transport characteristics of hyporheic zones (HZs). We use a simple and robust conceptualization of single peak flow events for a series of periodic sinusoidal bedforms. Using the model, we estimate the spatial extent of the HZ, the total amount of exchange, and the residence time of water and solutes within the reactive environment and its duration relative to typical time scales for oxygen consumption (i.e., a measure of the denitrification potential). Our results demonstrate that HZ expansion and contraction is controlled by events yet modulated by ambient groundwater flow. Even though the change in hyporheic exchange flux (%) relative to baseflow conditions is invariant for different values of channel slopes, absolute magnitudes varied substantially. Primarily, peak flow events cause more discharge of older water for the higher aspect ratios (i.e., for dunes and ripples) and lower channel slopes. Variations in residence times during peak flow events lead to the development of larger areas of potential nitrification and denitrification in the HZ for longer durations. These findings have potential implications for river management and restoration, particularly the need for (re)consideration of the importance of hyporheic exchange under dynamic flow conditions.

1. Introduction

1.1. Functional Significance of Groundwater-Surface Water Interactions in the Hyporheic Zone

Hyporheic exchange flows occurring at the sediment-water interface (SWI) are characterized by continuous, bidirectional exchange of water, solutes, and energy between the river's main channel and its surrounding sediments (Gomez-Velez et al., 2014; Tonina & Buffington, 2011). This exchange process has been found to control biogeochemical cycling (Boano et al., 2014; Cardenas, 2015; Krause et al., 2013; Pinay et al., 2015), regulate stream temperature (Hannah et al., 2009; Krause, Hannah, & Blume 2011; Packman et al., 2004) and impact ecological functioning (Boulton et al., 1998; Brunke & Gonser, 1997; Harvey & Gooseff, 2015) along river corridors. Mechanistic understanding of dynamic hyporheic processes requires detailed knowledge of the interplay between drivers and controls for exchange such as dynamics in discharge, streambed morphology, sediment hydraulic conductivity and porosity, ambient groundwater flow, channel sinuosity, planform morphology, and channel geometry and slope (Boano et al., 2006; Gomez-Velez et al., 2014; Krause, Hannah, Fleckenstein, et al.,2011; O'Connor & Harvey, 2008; Stonedahl et al., 2010). These complex interactions and exchange mechanisms play a key role in influencing the magnitude of hyporheic exchange flux (HEF), residence time of water and solutes in the streambed, and the location of stagnation zones. As a consequence, the area and depth in the streambed (see Figure 1) exposed to variations in physical, chemical, and biological processes is also affected (Gomez et al., 2012; Gomez & Wilson, 2013; Gomez-Velez et al., 2017; Kaufman et al., 2017; Krause, Hannah, Fleckenstein, et al., 2011; Zarnetske et al., 2011).

1.2. Drivers and Controls of Hyporheic Exchange

Hyporheic exchange occurs over a wide range of spatial and temporal scales (Boano et al., 2014; Cardenas, 2015; Krause, Hannah, Fleckenstein, et al., 2011), ranging from millimeter-scale eddies that transfer

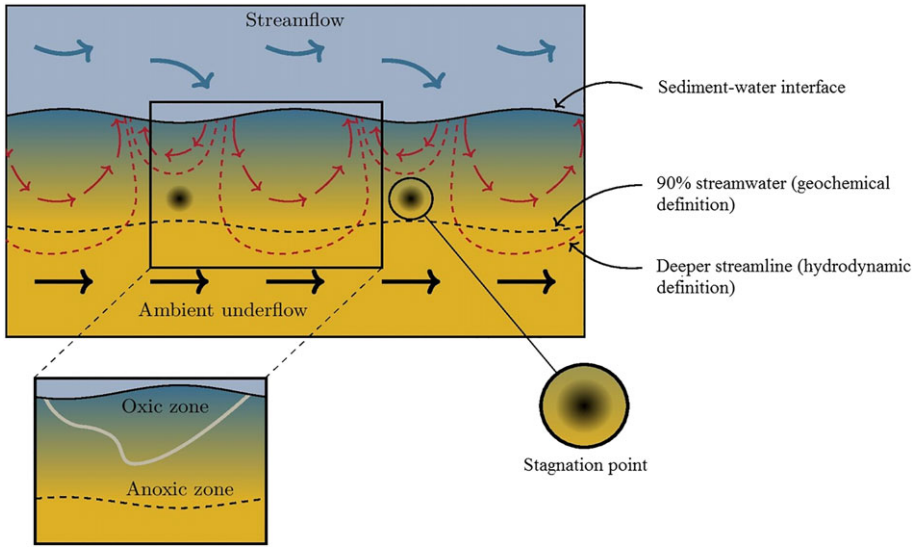

Figure 1. Conceptual sketch for the exchange processes. This image depicts the hydrodynamic (red dashed line depicting deeper streamline) and biogeochemical (black dashed line depicting biogeochemically active region with 90% of stream water) definitions of the hyporheic zones, the location of stagnation points, and the transition boundary (gray line) from oxic to anoxic zones during peak flows. These characteristics vary in space and time due to discharge dynamics.

momentum and solutes into the streambed over a few seconds to kilometer-scale flow paths along meander bends that exchange mass and solutes over time scales of decades and longer. The exchange process is driven by the spatial and temporal variations in the pressure distribution along the SWI, which is a function of discharge, channel geometry and slope, and streambed topography (Boano et al., 2014; Buffington & Tonina, 2009; Tonina & Buffington, 2009a; Wondzell & Swanson, 1999). At the same time, the exchange process is controlled by the sediment hydraulic properties and their heterogeneity (Gomez-Velez & Harvey, 2014; Ryan & Boufadel, 2006) and the ambient groundwater flow (Buffington & Tonina, 2009; Cardenas et al., 2004).

1.3. Influence of Transient Stream Flow on Hyporheic Exchange

While the aforementioned drivers and controls for hyporheic exchange have been intensively studied over the last three decades, particularly for steady state flow conditions (Buffington & Tonina, 2009; Cardenas et al., 2004; Tonina & Buffington, 2009b), we are only starting to understand the importance of transience in stream flow (Boano et al., 2007; Gomez-Velez et al., 2017; Malzone, Lowry, et al.,2016; Schmadel et al., 2016; Tonina & Buffington, 2011; Trauth & Fleckenstein, 2017). Time variance in stream flow can result from natural variation of precipitation inputs, evapotranspiration or snowmelt as well as from anthropogenic activity in wastewater treatment plants or dam operations, which can lead to effects such as hydropeaking and thermal peaking. During peak flow events, the potential for enhanced surface water downwelling, which is usually richer in oxygen, dissolved organic matter, and nutrients, can impact the type and rates of streambed biogeochemical processes including aerobic and anaerobic carbon respiration, nitrification, and denitrification (Gu et al., 2008; Harvey et al., 2013; Trauth & Fleckenstein, 2017). Moreover, surface water-borne contaminants along with the water and other solutes may be transported into the streambed (Fritz & Arntzen, 2007), potentially reaching greater depths and larger streambed areas (Figure 1; Bruno et al., 2009, 2013; Casas-Mulet et al., 2015; Jones, 2014). Consequently, fluctuations in stream stage and flow can effect benthic invertebrates, nutrient cycling, and thermal conditions in hyporheic and benthic environments (Bruno et al., 2013; Casas-Mulet et al., 2015; Jones, 2014; Sawyer et al., 2009).

Recent studies have shown the importance of understanding the dynamic nature of river corridors (Boano et al., 2013; Dudley-Southern & Binley, 2015; Gomez-Velez et al., 2017; Malzone, Anseeuw, et al., 2016; Malzone, Lowry, et al., 2016; McCallum & Shanafield, 2016; Schmadel et al., 2016; Trauth & Fleckenstein, 2017; Ward et al., 2013; Ward et al., 2018) and identified dominant drivers and controls of hypoheic exchange flows during transient stream flow conditions. For example, Malzone, Lowry, et al. (2016) showed that the annual and storm-induced groundwater fluctuations is the key control on the volume of HZ and Schmadel et al. (2016) highlighted the importance of controls such as hillslope lag, amplitude of the hillslope, and cross-valley

and down-valley slopes on hyporheic flow path and residence times. McCallum and Shanafield (2016) found alterations in the residence time distributions of bank inflows and outflows for different discharge events. Trauth and Fleckenstein (2017) highlighted the importance of peak discharge and duration of the events on the mean age of the water and solutes, which lead to higher rates of aerobic and anaerobic respiration. In the most recent work by Gomez-Velez et al. (2017), the authors explored the combined role of flow characteristics with varying channel planimetry, channel gradient, and morphology on the spatial and temporal evolution of river bank storage and sinuosity-driven hyporheic exchange using a dimensionless framework. However, none of the previous dynamic studies integrated the hydrological and geomorphorhic controls of hypoheic exchange flows with biogeochemical potential systematically.

1.4. Aims and Objectives

In this paper, we provide a systematic approach to decipher the potential impacts of transient forcing on hypoheic exchange flows, using reduced-order models of idealized, uniform, and single type of bedform-induced hyporheic exchange. Here we use the term *reduced-order* to emphasize that the model formulation only attempts to capture first-order drivers and controls of the exchange process, ignoring some of the complexities such as heterogeneity and coupling of turbulent flow in the water column with groundwater flow in the sediment. These assumptions allow us to gain comprehensive understanding from many simulations. Using reduced-order models, we explore a comprehensive parameter space and perform sensitivity analyses in order to identify the range of possible impacts by considering alterations of stream bedform geometries, channel gradient, peak flow characteristics, and biogeochemically relevant residence time scales in different bedforms like ripples, dunes, and alternating bars. In addition to HEF, we analyze hyporheic residence time distributions to quantify potential biogeochemical implications of time-varying stream flow. We therefore introduce a novel metric, the HZ efficiency for different time scales for oxygen consumption (using a definition of the Damköhler number similar to Gomez-Velez et al., 2015; Ocampo et al., 2006; Pinay et al., 2015; Zarnetske et al., 2012).

2. Methods

2.1. Conceptual Model

We use a simple conceptualization to explore the role of flow dynamics on the characteristics of bedform-induced hyporheic exchange. For simplicity, we assume that the bedforms are stationary and their shape and hydraulic properties are unaffected by changes in river discharge. Our modeling domain (Ω in Figure 2) represents stream sediments with a sinusoidal SWI ($\partial\Omega_{SWI}$) as the idealized small-scale topography is often represented by sinusoidal structure in the downstream direction (Stonedahl et al., 2010). The functional form of the SWI is given by $Z_{SWI} = (\Delta/2)\sin(2\pi x/\lambda)$, where Δ (L) and λ (L) are the characteristic amplitude and wavelength of the bedforms (e.g., ripple, dune, and riffle-pool sequences), respectively. The total streamwise length and depth of the modeling domain are $L = 3\lambda$ and d_b (L), respectively, and were selected to avoid boundary effects in the numerical simulations (see Table 1 for the values used in the model). Within this domain, we implemented a detailed flow and transport model using COMSOL Multiphysics. The finite element mesh consists of triangular elements with a maximum size of 0.05λ and with telescopic refinement of 0.0125λ along the SWI ($\partial\Omega_{SWI}$) and lateral boundaries ($\partial\Omega_u$ and $\partial\Omega_d$), resulting in a total of about 56,500 elements. This level of refinement is needed for mesh-independent simulations and to capture the effect of local, fast-flowing hyporheic circulation cells and calculate accurate boundary fluxes.

2.2. Flow Model

Neglecting the storage term, a reasonable assumption for submerged channel sediments, flow within the domain is described by the following version of the groundwater flow equation and Darcy's law:

$$\nabla \cdot \left[\rho \frac{\kappa}{\mu}(\nabla p + \rho g \nabla z)\right] = 0, \tag{1}$$

where $\mathbf{x} = (x, y)$ is the spatial location vector (L), $p(\mathbf{x}, t)$ is pressure ($M{\cdot}L^{-1}{\cdot}T^{-2}$), g is the acceleration due to gravity (L/T^2), κ is the permeability (L^2), ρ is fluid density (M/L^3), μ is fluid dynamic viscosity ($M{\cdot}L^{-1}{\cdot}T^{-1}$), $h = \frac{p}{\rho g} + z$ is hydraulic head (L), and Darcy velocity is $\mathbf{q} = -\frac{\kappa}{\mu}(\nabla p + \rho g \nabla z)$ (L/T).

Flow is driven by pressure gradients at the SWI ($\partial\Omega_{SWI}$). For simplicity, we use a prescribed head distribution that assumes a linear combination of head fluctuations induced by large- and small-scale bed topography (Stonedahl et al., 2010; Wörman et al., 2006):

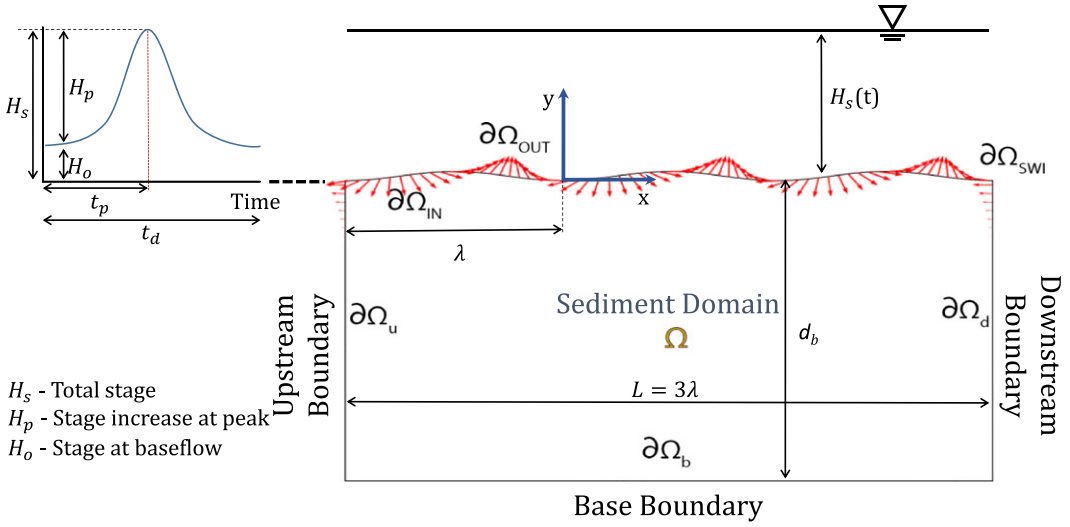

Figure 2. Depiction of the reduced-order model. Hyporheic exchange is induced by the interaction of stage variations with the bedform topography. The sediment domain (Ω) is assumed homogeneous and isotropic. A prescribed head distribution is imposed along the SWI ($\partial\Omega_{SWI}$), which can be further discretized into inflow ($\partial\Omega_{IN}$) and outflow boundaries ($\partial\Omega_{OUT}$) (red arrows). Periodic boundary conditions are assumed for the lateral boundaries ($\partial\Omega_u$ and $\partial\Omega_d$), horizontal ambient flow is assumed proportional to the channel slope, and the base of the model domain ($\partial\Omega_b$) is assumed impervious. SWI = sediment-water interface.

$$h_{SWI}(x,t) = -Sx + [H_s(t) - Z_{SWI}(x)] + \frac{2\,h_d(t)}{\Delta} Z_{SWI}\left(x + \frac{\lambda}{4}\right), \tag{2}$$

where S is channel slope, $H_s(t)$ (L) is the time-varying river stage, $Z_{SWI}(x)$ is the function describing the bed topography, and $h_d(t)$ is the intensity of the dynamic head fluctuations (Elliott & Brooks, 1997)

Table 1
Parameterization of the Numerical Model for the Analysis

Parameters	Value	Description
Constant model parameters		
d_b	5 m	Depth of the domain
B	5 m	Channel width
M	0.05	Manning's coefficient
α_L	0.05 m	Longitudinal dispersivity
α_T	0.005 m	Transverse dispersivity
κ	10^{-10} m^2	Permeability
ρ	1,000 kg/m^3	Fluid density
μ	1.002×10^{-3} Pa·s	Fluid dynamic viscosity
g	9.81 m/s^2	Acceleration due to gravity
d_{bkf}	$10^2 \times \Delta$ m	Bankfull depth
H_0	$0.1 \times d_{bkf}$	Reference stage
Varied model parameters		
Δ/λ	0.1, 0.01, and 0.001	Bedform aspect ratio
S	0.1, 0.01, 0.001, and 0.0001	Channel slope
H_p	$50\% \times d_{bkf}$ and $100\% \times d_{bkf}$	Peak stage
t_d	1 and 10 days	Duration of the peak flow event
t_p/t_d	0.25 and 0.5	Flow skewness
τ_{o_2}	0.5, 1, and 10 hr	Time scale for oxygen consumption

$$h_d(t) = 0.28\frac{U_s(t)^2}{2g}\begin{cases}\left(\frac{\Delta}{0.34\,H_s(t)}\right)^{3/8} & \text{for } \frac{\Delta}{H_s(t)} \leqslant 0.34\\ \left(\frac{\Delta}{0.34\,H_s(t)}\right)^{3/2} & \text{for } \frac{\Delta}{H_s(t)} > 0.34\end{cases}, \tag{3}$$

where the mean velocity is estimated with the Chezy equation for a rectangular channel as $U_s(t) = M^{-1}H_s(t)^{2/3}S^{1/2}$ with M as the Manning coefficient ($L^{-1/3}\cdot T$; Dingman, 2009). Notice that the pressure distribution at the SWI is the function of both space x and time t, where the temporal fluctuations are induced by the peak flow event (see section 2.2.1).

Assuming that bedforms repeat periodically along the channel, we implemented a periodic boundary condition for the lateral boundaries ($\partial\Omega_u$ and $\partial\Omega_d$; $p(x=-L,y,t) = p(x=2L,y,t) + \rho g[h_{SWI}(x=-L,t) - h_{SWI}(x=2L,t)]$). Under neutral groundwater conditions (i.e., without gaining and losing groundwater conditions), the only groundwater flow constraining the HZ is the ambient groundwater flow driven by the channel gradient (i.e., horizontal underflow component), and therefore, no flow is assumed for lower boundary ($\partial\Omega_b$). The depth of this boundary (d_b) was selected to minimize boundary effects. Finally, the solution under steady state (i.e., baseflow conditions) is used as the initial condition for the transient simulations (i.e., during the peak flow event). This method of calculating pressure distribution at the SWI reproduces reasonable observations. It also allows the exploration of large number of scenarios with fewer complexities when implemented in the model and with reduced computational demands.

The SWI ($\partial\Omega_{SWI}$) can be discretized into inflow ($\partial\Omega_{IN} = \{\mathbf{x} \mid (\mathbf{n}\cdot\mathbf{q} < 0) \wedge (\mathbf{x} \in \partial\Omega_{SWI})\}$) and outflow subboundaries ($\partial\Omega_{OUT} = \{\mathbf{x} \mid (\mathbf{n}\cdot\mathbf{q} > 0) \wedge (\mathbf{x} \in \partial\Omega_{SWI})\}$) such that $\partial\Omega_{SWI} = \partial\Omega_{IN} \cup \partial\Omega_{OUT}$ (see Figure 2) with $\mathbf{n}$ an outward vector normal to the boundary. Notice that these boundaries are dynamic in nature, contracting and expanding with variations in the forcing.

2.2.1. Hydrograph Generation

A single peak flow pulse is used to mimic the dynamic nature of river discharge (Figure 2). This transient hydrologic forcing changes the HZ's flow field, spatial extent (area and depth) and residence times (Gomez-Velez et al., 2017; McCallum & Shanafield, 2016; Wondzell & Swanson, 1999), having potentially important implications for biogeochemical transformations. The deterministic stage hydrograph was modeled with an asymmetric curve previously proposed by Cooper and Rorabaugh (1963):

$$H_s(t) = \begin{cases} H_0 + H_p\, e^{-\delta(t-t_p)\,\frac{[1-\cos(wt)]}{[1-\cos(wt_p)]}} & \text{if } t \in [0, t_d],\\ H_0 & \text{otherwise,}\end{cases} \tag{4}$$

where H_0 is the stage at baseflow conditions (L), H_p is the maximum rise of stream stage (L), t_p is the time to peak of the event (T), t_d is the duration of the peak flow event (T), $w = 2\pi/t_d$ is the frequency of the event (T^{-1}), and $\delta = w\cot(wt_p/2)$ is a constant that determines the degree of asymmetry (T^{-1}).

2.3. Solute Transport Model and Delineation of the Hyporheic Zone

The advection-dispersion equation is used to model the transport of conservative solutes within the sediments

$$\theta\frac{\partial C}{\partial t} = \nabla\cdot(\mathbf{D}\nabla C) - \nabla\cdot(\mathbf{q}C), \tag{5}$$

where C is concentration (M/L^3), $\mathbf{q}$ is the Darcy flux (L/T), and $\mathbf{D} = \{D_{ij}\}$ is the dispersion-diffusion tensor defined as (Bear, 1972)

$$D_{ij} = \alpha_T|\mathbf{q}|\delta_{ij} + (\alpha_L - \alpha_T)\frac{q_i\,q_j}{|\mathbf{q}|} + \frac{\theta}{\xi_m}D_m, \tag{6}$$

with α_T and α_L the transverse and longitudinal dispersivities (L), D_m is the effective molecular self-diffusion coefficient, $\xi_m = \theta^{-1/3}$ is the fluid tortuosity (defined here with the Millington & Quirk, 1961, model), and δ_{ij} is the Kronecker delta function.

Modeling the transport of a conservative tracer allows us to explore the mixing and extend of the HZ. We assume that the concentration of the tracer in the stream water column is C_s, and therefore, a prescribed boundary condition $C(\mathbf{x},t) = C_s$ is used along the SWI's inflow areas ($\partial\Omega_{IN}$). Outflow areas ($\partial\Omega_{OUT}$) along the SWI are advective boundaries where $\mathbf{n}\cdot(\mathbf{D}\nabla C) = 0$. Lateral boundaries ($\partial\Omega_u$ and $\partial\Omega_d$) are periodic boundaries $C(x=-L,y) = C(x=2L,y)$, and the bottom boundary ($\partial\Omega_b$) is a no-flow boundary $\mathbf{n}\cdot(\mathbf{q}C - \mathbf{D}\nabla C) = 0$. An initial condition for the concentration field is obtained from a steady state simulation of the transport model (equation (5)) under baseflow conditions (i.e., $H_s = H_0$). In this case, the HZ is defined as the zone with at

Table 2
Description of the Peak Flow Event Scenarios Used for the Analysis

No.	Scenario	Event duration (day)	Skewness	Peak flow intensity (percent of d_{bkf})
1	$FD_{low}Sk_{low}FI_{low}$	1	0.25	50%
2	$FD_{low}Sk_{low}FI_{high}$	1	0.25	100%
3	$FD_{low}Sk_{high}FI_{low}$	1	0.5	50%
4	$FD_{low}Sk_{high}FI_{high}$	1	0.5	100%
5	$FD_{high}Sk_{low}FI_{low}$	10	0.25	50%
6	$FD_{high}Sk_{low}FI_{high}$	10	0.25	100%
7	$FD_{high}Sk_{high}FI_{low}$	10	0.5	50%
8	$FD_{high}Sk_{high}FI_{high}$	10	0.5	100%

Note. FD = peak flow event duration; Sk = peak flow skewness; FI = peak flow intensity; d_{bkf} = bankfull depth.

least 90% of the pore water originated from the stream (i.e., $C \geq 0.9C_s$). This definition is similar to the one proposed by Triska et al. (1989) and Gomez-Velez et al. (2014, 2017). Through the manuscript, we refer to this definition as the *biogeochemical definition of the HZ*.

2.4. Residence Time Model

The HZ residence time describes the time that water and solutes are exposed to the stream sediment biogeochemical conditions. Here we evaluate the impacts of transient flow, driven by a peak flow event, on the moments of the HZ's residence time distribution. To this end, we use the approach outlined in Gomez et al. (2012) Gomez and Wilson (2013), and Gomez-Velez et al. (2017) where the moments of the residence time distribution are described by an advection-dispersion equation of the form

$$\frac{\partial(\theta a_n)}{\partial t} = \nabla \cdot (\theta \mathbf{D} \nabla a_n) - \nabla \cdot (\mathbf{v}\theta a_n) + n\theta a_{n-1}, \tag{7a}$$

$$a_n(\mathbf{x}, t) = 0 \quad \text{on } \partial\Omega_{IN}, \tag{7b}$$

$$\mathbf{n} \cdot (\theta \mathbf{D} \nabla a_n) = 0 \quad \text{on } \partial\Omega_{OUT}, \tag{7c}$$

$$a_n(x = -L, y) = a_n(x = 2L, y) \text{ for } \partial\Omega_u \text{ and } \partial\Omega_d, \tag{7d}$$

$$\mathbf{n} \cdot (\mathbf{q}a_n - \mathbf{D}\nabla a_n) = 0 \quad \text{on } \partial\Omega_b, \tag{7e}$$

$$a_n(\mathbf{x}, t = t_0) = a_{n0} = \int_0^\infty \xi^n \Psi_0(\mathbf{x}, \xi)\, d\xi, \tag{7f}$$

where $a_n(\mathbf{x}, t)$ (T) ($n = 1, 2, \ldots$ and $a_0(\mathbf{x}, t) = 1$) is the nth moment of the residence time distribution $\Psi(\mathbf{x}, t, \tau)$ (T^{-1}), which is defined as

$$a_n(\mathbf{x}, t) = \int_0^\infty \xi^n \Psi(\mathbf{x}, t, \xi)\, d\xi, \text{for } n = 1, 2, \ldots . \tag{8}$$

Initial and boundary conditions are defined following the approach in Gomez and Wilson (2013) and Gomez-Velez et al. (2017). Similar to the conservative transport model, the initial distribution of the first (mean residence time) and second (variance of residence time) moments were estimated under steady baseflow conditions.

2.5. Peak Flow Event Scenarios

Typical geomorphic length scales for ripples, dunes, and alternating bars in a broad range river sizes and hydraulic conditions were estimated with the methodology proposed by Gomez-Velez and Harvey (2014) and Gomez-Velez et al. (2015). This approach uses the best available empirical equations for length scales and a Monte Carlo approach to generate plausible scenarios that represent variations along a real river network (Gomez-Velez & Harvey, 2014). Our simulations explore three different values of bedform aspect ratio: ripples ($AR = 0.1$), dunes ($AR = 0.01$) and alternating bars ($AR = 0.001$) (Bridge, 2009; Dingman, 2009). For each of these bedforms we also explore (i) two flow skewness values (t_p/t_d): 0.25 and 0.5, where the latter value is typically observed in regulated systems, for example, reservoirs and sewage discharge (Sawyer et al., 2009), (ii) two peak flow intensities: 50% and 100% of typical bankfull depth (d_{bkf}), (iii) two values of event duration: 1 and 10 days, and (iv) four values of channel slope: 0.1, 0.01, 0.001, and 0.0001. This results in 96 scenarios; however, we focus our discussion on a handful of peak flow event scenarios, as shown in Table 2 and Figure 3. These scenarios allow us to systematically explore the effects of flow dynamics in the hyporheic exchange process.

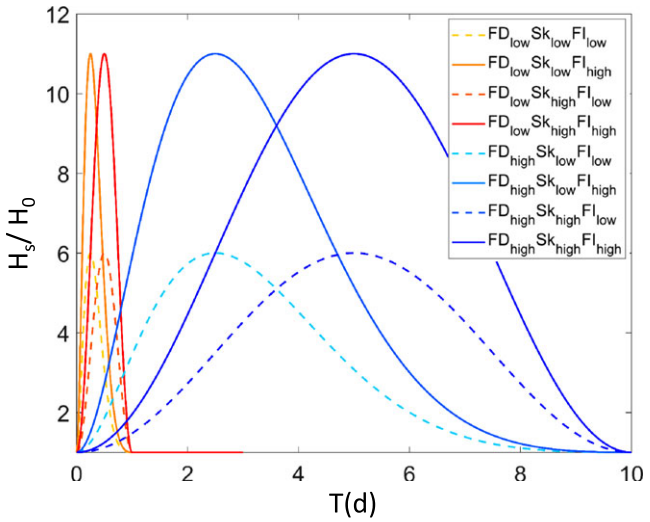

Figure 3. Depiction of the stage hydrographs produced by the equation (4) and associated with the scenarios shown in the Table 2.

2.6. Metrics

We use multiple metrics to quantify the impact of transient forcing in hyporheic exchange. In the following, we briefly define and describe each of them.

2.6.1. Hyporheic Zone Area and Penetration

Dynamic changes in the pressure distribution along the SWI induce changes in the sediment flow field and therefore in the extent (area and penetration depth) of the HZ, that is, the area of the sediment exposed to water originating from the stream. We estimate the boundary of the HZ using both a hydrodynamic and a biogeochemical criteria (Gooseff, 2010).

First, the hydrodynamic definition assumes that the HZ boundary corresponds to the deepest streamline originating and terminating in the SWI. The flow field, and therefore this boundary and area of the HZ, is highly sensitive to dynamic changes in hydrologic forcing. The high sensitivity is explained by the negligible porous media storage of the stream sediments, which results in a fast propagation of pressure fluctuations at the SWI (i.e., the response time is negligible). Second, the biogeochemical definition, similar to the one used by Gomez-Velez et al. (2014), assumes that the boundary of the HZs corresponds to the contour defining porewaters with 90% stream water. The other metrics below use the biogeochemical definition of the HZ in order to define the boundaries of integration.

2.6.2. HEF

The HEF corresponds to the integral of the Darcy flux along the sections of the SWI discharging hyporheic water into the stream:

$$Q_{hz,\mathrm{out}} = \frac{\int_{\partial\Omega_{\mathrm{out},hz}} n.q \, \mathrm{d}x}{\int_{\partial\Omega_{\mathrm{SWI}}} \mathrm{d}x}, \tag{9}$$

where $\partial\Omega_{\mathrm{out},hz}$ is the outflow boundary discharging hyporheic water, defined by the biogeochemical definition.

2.6.3. Residence Times

Similarly, a representative value of residence time for the exchange process is estimated by flux-weighting the modeled mean residence time, standard deviation of residence time (*SD*), and coefficient of variation of residence time (*CV*) along the sections of the SWI discharging hyporheic water into the stream. See section 2.4 for a detailed description of the residence time model. The mean residence time (μ) corresponds to the first central moment (a_1), the standard deviation of residence time is calculated as $\sigma = \sqrt{a_2 - \mu^2}$, with a_2 the second central moment, and finally *CV* is calculated as $\frac{\sigma}{\mu}$.

2.6.4. HZ Efficiency

Likely locations and size of the oxic-anoxic zones have been described by using the Damköhler number, $DN = a_1/\tau_{o_2}$, where τ_{o_2} is the biogeochemical time scale for oxygen consumption and its typical value varies from 0.5 to 10 hr (Gomez-Velez et al., 2015). *DN* allows us to explore and compare the role of reaction and transport

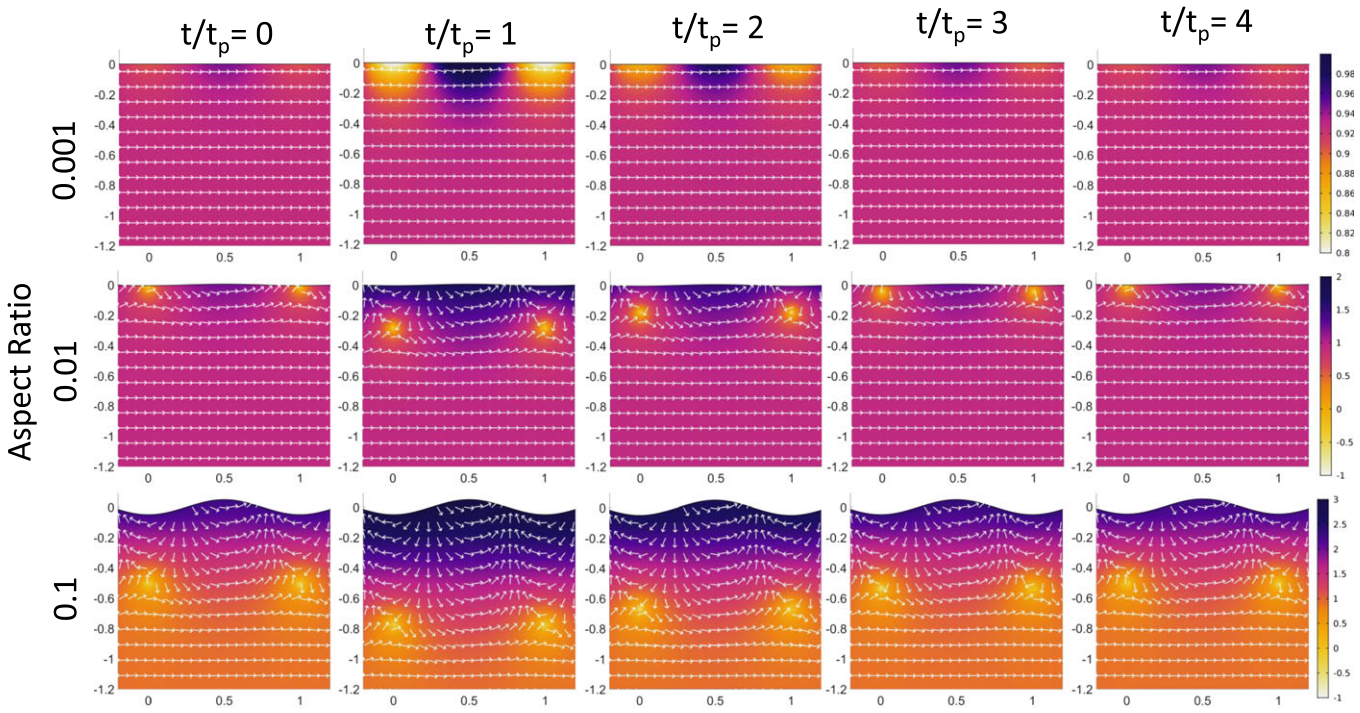

Figure 4. Snapshots of the flow field (white arrows represent direction and not proportional to magnitude) within the sediment at different times t/t_p. Colored surface represents the magnitude of Darcy flux vector in log scale m/d (white is low, and black is high). Rows correspond to different bedform aspect ratios: $AR = 0.001$ is typical for alternating bars, $AR = 0.01$ is typical for dunes, and $AR = 0.1$ typical for ripples. The scenarios include peak flow intensity of 50% of d_{bkf}. For all panels, the channel slope is 10^{-1} and the hydraulic conductivity is 9.8×10^{-4} m/s. Vertical and horizontal axis are scaled by the bedform wavelength.

processes within the system (Ocampo et al., 2006; Pinay et al., 2015). in particular, DN for O_2 is an important indicator of the potential for net nitrification or denitrification in the HZ (Zarnetske et al., 2012).

To evaluate the biogeochemical potential of HZs and how it changes as a function of time, we assume that the stream water column is dominant source of oxygen entering the sediments. Similar to Gomez-Velez et al. (2015), we assume that $DN = 4.6$ corresponds to a 99% reduction in the oxygen concentration, and therefore, the sediment area where $DN \geq 4.6$ is essentially anoxic and a likely location where denitrication takes place. Similarly, the locations with $DN < 4.6$ are oxic zones where the presence of oxygen is likely to promote nitrification. In this work, we explore $\tau_{o_2} = 0.5$, 1, and 10 hr. To emphasize on the quantification of anoxic waters discharged from the HZs, we also calculate Q_{anoxic}. This is defined as the amount of anoxic waters discharged from the HZs with respect to different time scales for oxygen consumption. As an example, for the $\tau_{o_2} = 10$ hr, Q_{anoxic} will be the anoxic waters discharged from the HZ with residence times of over 10 hr.

Finally, we define the HZ efficiency as the ratio of the HEF discharging anoxic water (Q_{anoxic}) and the total HEF ($Q_{hz,\text{out}}$)

$$HZ_{\text{eff}} = \frac{Q_{\text{anoxic}}}{Q_{hz,\text{out}}}. \tag{10}$$

3. Results

3.1. Hyporheic Flow Patterns and Geometry of the HZ

The flow field (magnitude and direction) changes dynamically as the peak flow event moves along the SWI. Figure 4 illustrates the temporal evolution of these changes by comparing the fields before the event (i.e., baseflow at $t \leq 0$) and during the event ($t \leq t_d$). The HZ initially expands during the rising limb of the event and then contracts during the recession returning to the initial baseflow conditions (columns 2–5 in Figure 4). The shape of the peak flow event determines the impact in the flow field, and at the same time, the magnitude of the changes are controlled by the bedform aspect ratio.

Under baseflow conditions ($t \leq 0$), the HZ for alternating bars ($AR = 0.001$, Figure 4) is very small, almost completely absent. This is explained by the compressing effect of the ambient flow (proportional to the channel

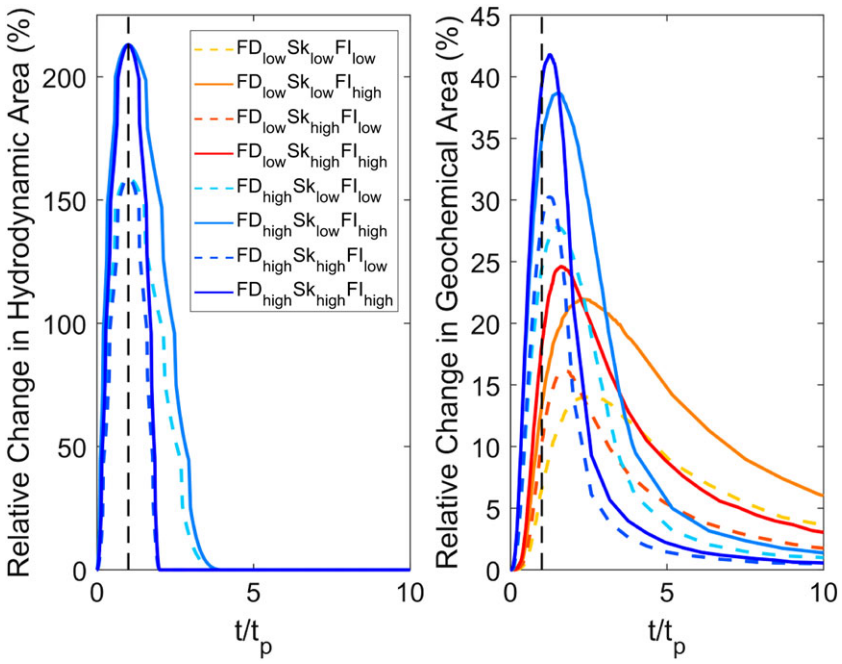

Figure 5. Relative change (to baseflow conditions) in hydrodynamic and biogeochemical hyporheic zone area (%) as a function of dimensionless time (t/t_p) for eight scenarios listed in Table 1. Channel slope and bedform aspect ratio are 10^{-1} and 0.01, respectively. Note that the curves associated with FD_{low} scenarios are coinciding with FD_{high} scenarios for the case of hydrodynamic area as it shows relative change.

slope). However, the peak flow event overcomes the moderating effect of the ambient flow and results in the emergence of a HZ that drastically penetrates into the sediments (Figure 4). On the other hand, morphologies with higher aspect ratios such as dunes ($AR = 0.01$) and ripples ($AR = 0.1$) consistently have a larger and more persistent HZ during the course of the event as illustrated in Figure 4.

These results highlight the importance of ambient groundwater flow (proportional to channel slope) and its moderating role under both steady and transient flow conditions. Figure 4 illustrates the case where the pressure gradient induced by bedform topography are not enough to overcome the modulating effect of the ambient flow. The magnitude of such gradients progressively increases during the event and eventually the hydrodynamic forcing overcomes the ambient groundwater flow, resulting in the development of a HZ (Figures 4b–4e). Moreover, higher peak flow intensities (FI_{high}) lead to an increase in vertical flow velocities, which produce a larger HZ and advect more mass into the streambed. This, at the same time, changes the location and size of stagnation zones, which oscillate in depth and size during the flow event, resulting in potential emergence of highly reactive environments purely driven by hydrodynamic changes. This is in line with the findings of Gomez and Wilson (2013). Note that the maximum extent of the HZ is always at peak flow; however, the evolution of the expansion and contraction strongly depends on the peak flow skewness (t_p/t_d) and peak flow magnitude.

3.1.1. Difference Between Hydrodynamic and Biogeochemical Extent of HZ Under Dynamic Flow Conditions

As discussed in section 2, HZ extent can be defined from a hydrodynamic and biogeochemical perspective. Each of these definitions represents different flow and transport processes and can have different sensitivities to transience. Our simulations show that these two definitions are not consistent under transient flow conditions. The relative change (to baseflow conditions) in hydrodynamic area (%) is considerably higher than the biogeochemical area (%) in response to different flow conditions (Figure 5). Notice that for the left panel, the curves associated with FD_{low} scenarios are coinciding with FD_{high} scenarios due to the scaling of time to the time to peak of the event. For scenarios with high peak flow intensity, the simulated hyporheic area based on the hydrodynamic definition increased by up to 200%, whereas the HZ area based on the respective biogeochemical definition is limited to 45% (for the slope value 10^{-1}). Note that both definitions result in the same area for steady flow, but the dynamic nature of the flow affects them differently. In particular, the biogeochemical definition, which is closely linked with transport and potential for biogeochemical transformations, tends

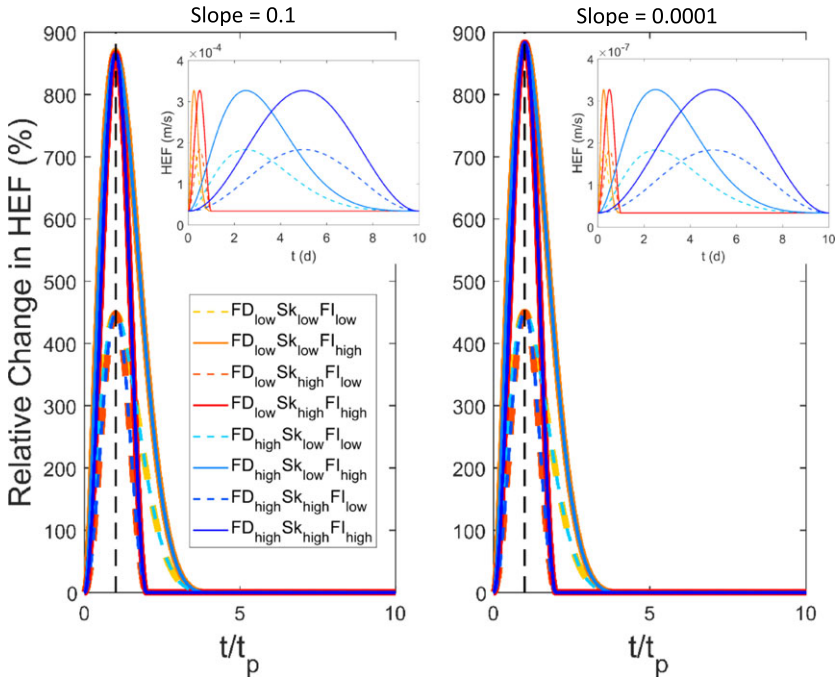

Figure 6. Relative change (to baseflow conditions) in net hyporheic exchange flux (%) as a function of dimensionless time (t/t_p) for eight scenarios listed in Table 1. The bedform aspect ratio is $AR = 0.01$, and the channel slopes are 10^{-1} and 10^{-4} for the left and right panels, respectively. Note that the curves associated with FD_{low} scenarios are coinciding with FD_{high} scenarios due to the scaling of time to peak of the event. For further clarification, insets in each panel show the evolution of exchange flux (m/s) as a function of time. HEF = hyporheic exchange flux.

to be more stable and relatively insensitive to transient forcing. In the case of the HZ's hydrodynamic area, the boundary used to estimate the area corresponds to the the deepest streamline that begins and ends at the SWI, which instantaneously mimics the pressure fluctuations at the interference. This area definition does not take into account the predominant mass transport and retention process within the HZ. The results shown here confirm that under dynamic flow conditions, the residence time and the length of hyporheic flow path may not be coupled (e.g., Schmadel et al., 2016; Ward et al., 2017). Furthermore, our simulations indicate that after the peak flow-induced expansion of the HZ area, there is a faster contraction of the hydrodynamically defined HZ; however, biogeochemically defined HZ takes longer time to return back to preevent conditions.

3.2. Impact of Transient Forcing on Net HEF and Residence Time

3.2.1. Net HEF

We quantify the change in net HEF, relative to baseflow conditions, for different scenarios and channel slopes (see Figure 6). Given the instantaneous hydraulic response time (Boano et al., 2007) of submerged sediments (implicit in equation (1)), the exchange flux and hydrograph are concurrent, resulting in the highest exchange differences at peak flow (t_p). Relative differences are notable, reaching values between 450% and 900% during peak flow, with the smaller differences for high channel slopes, as expected given the modulating effect of ambient groundwater flow.

Although the relative change (to baseflow conditions) in HEF (%) is invariant for both the scenarios, that is, for slope values 10^{-1} and 10^{-4}, the absolute numbers differ. Notice that for both the panels the curves associated with FD_{low} scenarios are coincident with FD_{high} scenarios due to the scaling of time to peak of the event, and hence, subsets depict evolution of exchange flux (m/s) as a function of time. For channel slopes of 10^{-1}, the absolute HEF is 3.27×10^{-4} m/s, whereas for slopes 10^{-4} is 3.27×10^{-7} m/s. These results highlight the impact of slope, that is, the channel gradient which drives the ambient flow in the streambed. HEF is generally greater in magnitude for slope value 10^{-1} as the channel gradient drives the horizontal flow with higher velocities resulting in higher rates of hyporheic waters discharged to the surface water.

3.2.2. Moments of the Residence Time Distributions

Ambient groundwater flow, which is proportional to the channel slope S, strongly modulates the residence time distributions for all bedform aspect ratios and forcing scenarios. First, systems with high channel slopes

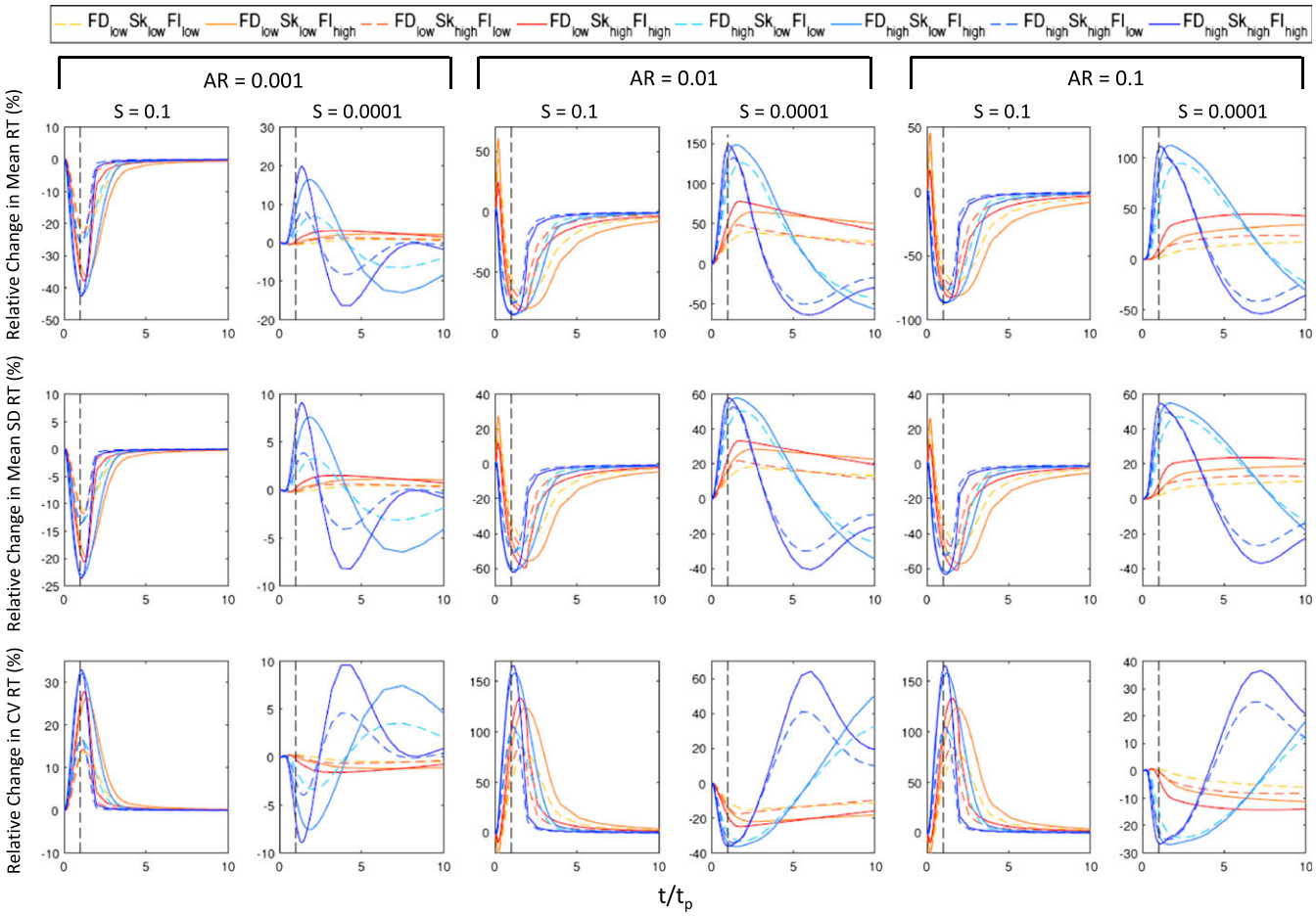

Figure 7. Relative Change (%) (to baseflow conditions) in mean residence time (RT), standard deviation of RT (SD RT), and coefficient of variation of RT (CV RT) as a function of dimensionless time (t/t_p) for eight scenarios listed in Table 1. Columns correspond to different bedform aspect ratios (0.001, 0.01 and 0.1) and channel slope values (10^{-1} and 10^{-4}).

are strongly modulated by the ambient groundwater flow, and therefore, the HZ cannot expand considerably during the peak flow event, forcing all the flow through relatively shallow flow paths and resulting in residence times with younger waters and less variability (see columns 1, 3, and 5 in Figure 7). On the other hand, low channel slopes allow the HZ to expand, penetrating deeper and discharging waters progressively older and with more variable residence times initially, reaching a maximum after the event's time to peak, and then switching to younger waters over the long term, where eventually the system returns to the original state (see columns 2, 4, and 6 in Figure 7). This is consistent with previous findings by Gomez-Velez et al. (2017) in the context of alluvial aquifers. Notice that this oscillatory behavior on the moments of the residence time distribution is attenuated for the events with low duration (FD_{low}, yellow, orange, and red lines in Figure 7). Note that unlike the exchange fluxes, the differences in the moments of the residence time distribution are lagged relative to the peak flow event (i.e., peak flow intensity and peak differences are reached at different times) and the return to baseflow conditions is relatively slow, specially as the flow duration is smaller and the skewness is higher. This is important from the perspective of solute retention within the reactive environment and the enhancement of transformations or slow release of contaminants.

Our simulation results for bedform aspect ratio of 0.01 reveal that for shorter event durations larger quantities of older water is released out of the SWI for higher slopes, that is, 10^{-1} (column 3 in Figure 7). This indicates that sudden penetration of larger quantities of surface water into deeper subsurface flow paths causes more discharge of older water even though for very short period of time. Moreover, for all the peak flow scenarios we observe discharge of younger hyporheic waters since steep slopes promote stronger ambient groundwater flow and hence causing compressing of HEF cells. In contrast, for low slopes (10^{-4}), the relative change (to baseflow conditions) in mean residence time (%) shows more discharge of older water during the event for

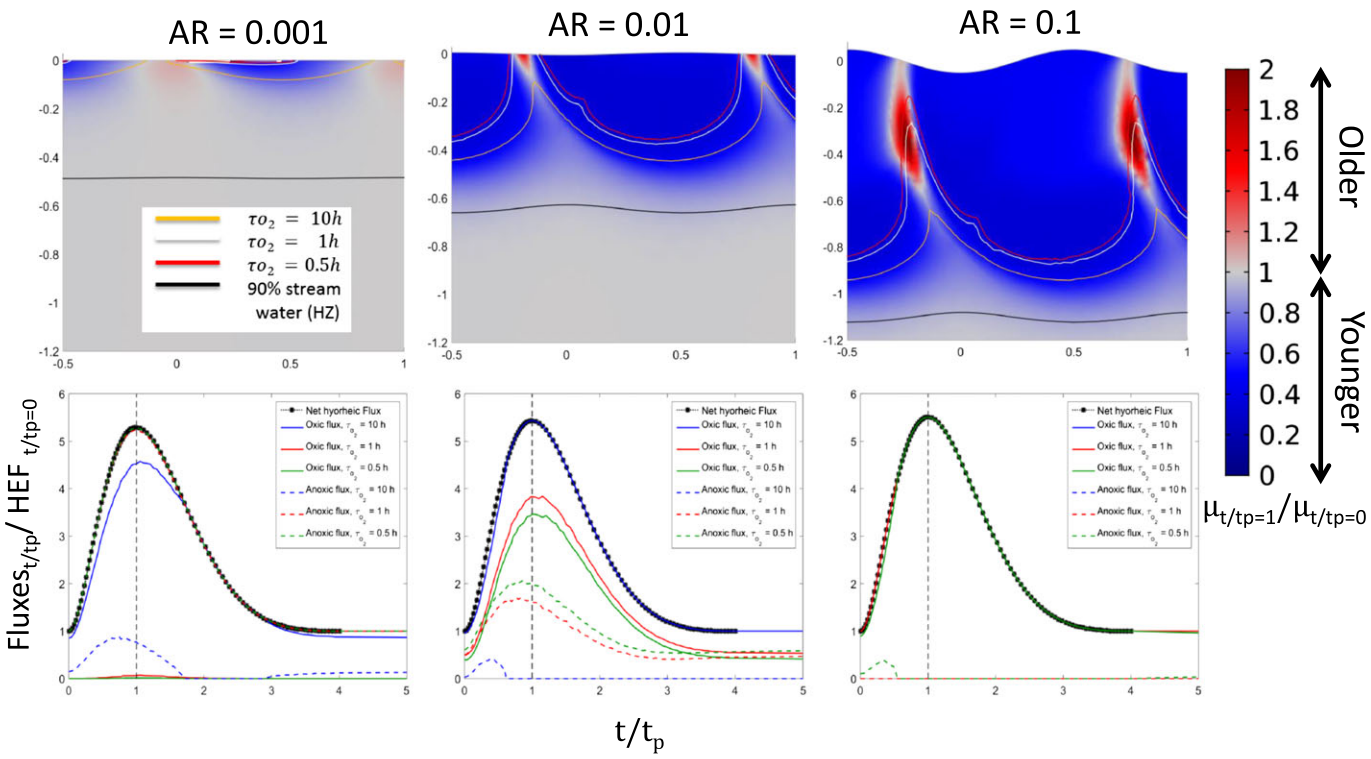

Figure 8. Snapshots for the ratio of mean residence time and the baseflow mean residence time at $t/t_p = 1$ (first row) and ratio of evolution of fluxes (net hyporheic exchange flux, oxic, and anoxic) and net hyporheic flux at $t/t_p = 0$ as a function dimensionless time (t/t_p; second row) for bedform aspect ratios 0.001, 0.01, and 0.1 (columns). Contours and curves correspond to the oxic-anoxic transition boundary for oxygen consumption time scales τ_{o_2} = 10, 1, 0.5 (hr). Extent of the HZ is based on the biogeochemical definition. Channel slope is 10^{-1} in all cases, and the vertical and horizontal axis are scaled by the bedform wavelength. HEF = hyporheic exchange flux; HZ = hyporheic zones.

all eight considered peak flow scenarios (highest $\approx$ 150%). This is due to the slow horizontal velocities of the ambient groundwater flow observed for low slopes, allowing HEF to penetrate the streambed at greater depths. These deeper and hence longer flow paths lead to broader residence time distributions.

Streambed topography also plays a dominant role in modulating the residence time of the water and the solutes in the streambed. For different bedform aspect ratios of the streambed the spatial distribution of the hydraulic head vary at the SWI. In the case of the aspect ratios of 0.001, due to the shallow fast flowing subsurface flow paths, there is particularly higher discharge of younger water as the stream stage rises and progresses back to initial conditions relatively quickly. Notice that, this is the case for all bedform aspect ratios but for the scenarios associated with shorter duration of the event and higher slope values (see columns 1, 3, 5 in Figure 7). However, if the event duration is longer, for the higher aspect ratios (see columns 3 and 5 in Figure 7), we observe relatively higher discharge of older waters after the sudden increase in the stream stage. However, for lower slope values, we observe long-term memory effects due to the slow horizontal ambient groundwater flows in the sediment domain. As presented in Figure 4, higher aspect ratios enlarges the HZ and elongates the subsurface flow paths in the streambed leading to higher discharge of older water. This indicates long-term release of older water postflow event, particularly for the events with longer duration, which implies that if there is a second peak (or multiple peaks) before the system has recovered to baseflow conditions, system will result with additional older waters, potentially providing more time for reactions and transformations.

For all the considered scenarios, we observe that the higher peak flow intensities (FI_{high}) intensify the impacts for the three metrics (Figure 7), that is, in contrast to lower peak flow intensities (FI_{low}). For example, focusing on bedform aspect ratio of 0.01, slope value of 10^{-4}, and shorter event duration, relative change (to baseflow conditions) in mean residence time (%) rises by $\approx$ 70% for FI_{high} and only $\approx$ 40% for FI_{low} , indicating more discharge of older water for higher peak flow intensities. A similar trend is observed for the shorter duration of the event (FD_{low}). This demonstrates the importance of peak flow intensity and event duration on the mean

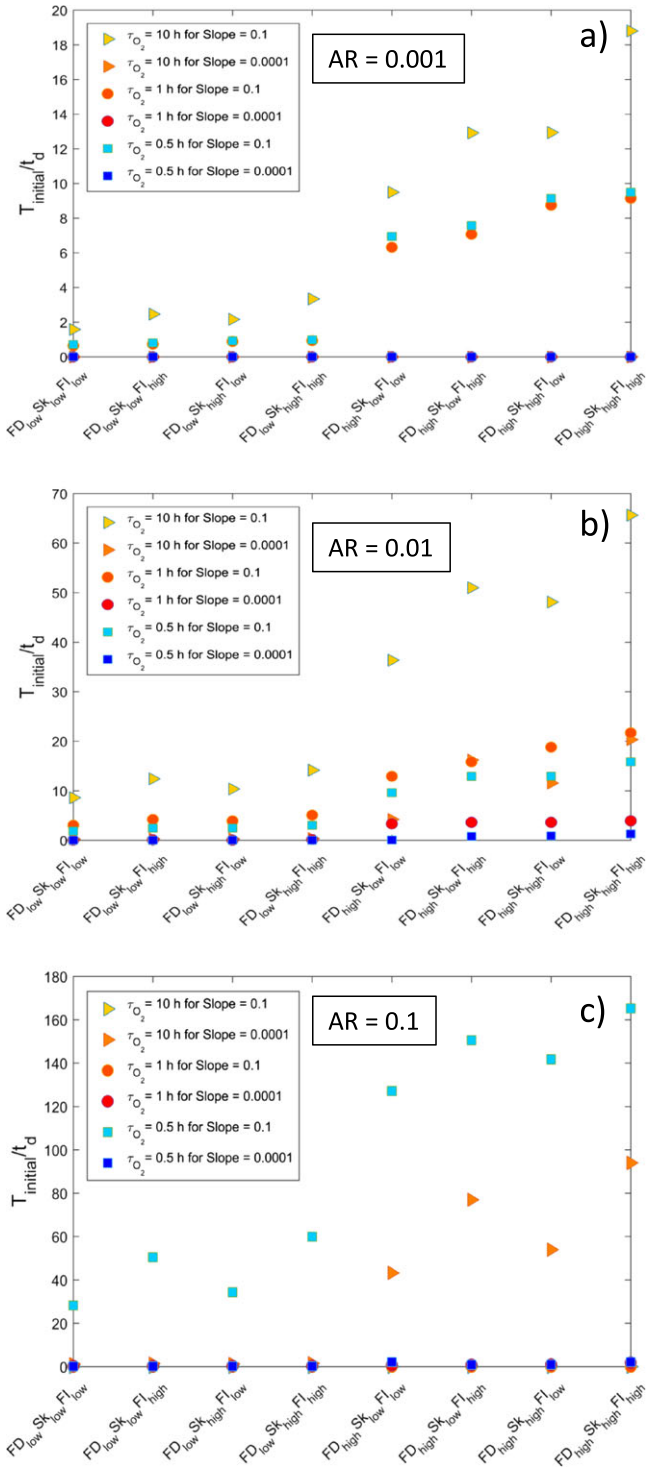

Figure 9. Hyporheic zones efficiency. Time to reach to the initial state of the system (i.e., to baseflow conditions) scaled to the duration of the peak flow event (t_d) for eight scenarios listed in Table 1 and three biogeochemical time scales for oxygen consumption (τ_{o_2} values = 10, 1, and 0.5 hr) and two channel slope values ($S = 10^{-1}$ and 10^{-4} for the bedform aspect ratios (a) 0.001, (b) 0.01, and (c) 0.1.

residence time (μ) of the water being discharged out of the SWI during and after a event. Therefore, each of the parameters involved in the simulations play a crucial role in determining the systems potential to discharge older or younger waters.

3.3. HZ Efficiency

We use the Damköhler number to delineate oxic and anoxic zones for various peak flow event and geomorphic scenarios—a proxy for the oxygen consumption and denitrification potential. The vertical penetration of both the HZ and the oxic-anoxic zone increases with bedform aspect ratio (Figure 8), highlighting the impact of channel topography in the transport of water and solutes within the streambed.

For bedform aspect ratio of $AR = 0.001$ cause only shallow oxic zones, that is, close to the SWI indicating occurrence of aerobic respiration only at the shallow regions of the streambed. However, during peak flow events there will be discharge of anoxic hyporheic waters from the streambed for all τ_{o_2} values (Figure 8). This indicates existence of favorable conditions for denitrification in the deepest hyporheic flow paths, which also relies on the availability of dissolved organic carbon (DOC) as an electron donor deep in the streambed. Whereas, for $AR = 0.01$, with a time scale for oxygen consumption being 10 hr, predominantly oxic hyporheic water is released from the SWI. This can be explained by the high flow velocities along the shallow subsurface flow paths resulting in younger water closer to the SWI. However, we also found that comparatively more anoxic water is released for lower τ_{o_2} values (i.e., 0.5 and 1 hr) for aspect ratio of 0.01 during the event. Moreover, for $AR = 0.1$, aerobic conditions extend deeper into the streambed during peak flows (Figure 8). It indicates that the anoxic hyporheic waters would remain in the streambed during the peak flows and eventually discharged after the recession of the event. It is important to notice that these results represent the higher channel slope value (10^{-1}) and that the interplay between the channel gradient and morphology varies the transport of oxygen into the streambed.

An analysis of potential memory effects of postevent (based on the metric-HZ efficiency) on the biogeochemical characteristics of the HZ and streambed environment has been performed using the example of nitrogen cycling. The time to reach the initial state of the system after a peak flow event increases with the duration of the event (see FD_{high} scenarios in Figure 9). This implies that conditions favoring denitrification are prevalent for longer time; hence, the nitrate removal efficiency of the system could be potentially higher. During longer events, reaction times would be substantially enhanced primarily for $AR = 0.01$ and $AR = 0.1$ (see Figures 9b and 9c). Furthermore, event characteristics such as skewness of flow peaks and intensities have substantial impact on the simulated HZ efficiency. For instance, we observe that the Fl_{high} scenarios result in higher $T_{initial}/t_d$ than Fl_{low} scenarios. Moreover, higher peak flow skewness causes higher $T_{initial}/t_d$ even though the impact of peak flow skewness is not as pronounced as seen for event duration and peak flow intensity (Figure 9).

4. Discussion

4.1. Dynamic HZ Expansion, Contraction, and Exchange Fluxes

Recent studies have recognized the need for comprehensive studies on the drivers and controls of hypoheic exchange (Malzone, Lowry, et al., 2016; McCallum & Shanafield, 2016; Schmadel et al., 2016); hence, we have attempted to present an integrated, comprehensive, and systematic approach that incorporates a wide range of parametric combinations. Our study combined both geomorphic (streambed topography and channel

gradient) and hydrological controls (different peak flow event characteristics like intensity and skewness of the peak and duration of the event) to gain mechanistic understanding of flow patterns and exchange fluxes between groundwater-surface water interfaces.

Our study showed that the increased pressure gradient at the SWI due to a peak flow event cause HZ appearance and then expansion, which was maximum at the peak flows indicating the dominance of transient driver on hypoheic exchange. However, on the basis of our further findings, it is evident that pressure distribution caused by the transient forcings is majorly counteracted by the ambient groundwater flow. Primarily, steeper channel slopes exert stronger underflow and compress the HZs. The importance of slopes of streambed on hyporheic exchange has been highlighted for steady state discharge conditions by Cardenas and Wilson (2006) and Tonina and Buffington (2009a).

Under transient discharge conditions, the HZ extent based on hydrodynamic and biogeochemical definitions varied drastically. We observed rapid changes in gradients during the course of the flood event, whereas the penetration of surface water solutes was decelerated by the counterdirectional nature of the local flow patterns. This in turn leads to the development of dynamic stagnation zones (i.e., zones with extremely low or zero velocities), where solutes might accumulate and develop regions of *biogeochemical hot spot* in the streambed (Gomez & Wilson, 2013).

4.2. Potential Impacts of Transient Forcing on Biogeochemical Processes

During high discharge conditions, the transport of surface water into the streambed accelerates (Gu et al., 2008; Malcolm et al., 2004), hence leading to increased accumulation of solutes deeper into the streambed. Previous research has demonstrated that the nutrient cycling at the river-aquifer system is strongly controlled by, and often proportional to the residence times of surface water in the HZ (McCallum & Shanafield, 2016; Wondzell & Swanson, 1999; Zarnetske et al., 2011, 2012) and are good indicators of biogeochemical processes (Sanz-Prat et al., 2015, 2016). Our results indicate that peak flow event characteristics like magnitude, skewness of peaks, and duration of the event can have a considerable impact on HEF and the mean residence time of water in the HZ. Stormflow-induced variability in HEF controls the transport of water and solutes (and even contaminants) deeper in the alluvium and alters its residence times in the streambed and hence may also impact rates of biogeochemical transformations (as shown by the results of Gomez & Wilson, 2013, and Trauth & Fleckenstein, 2017).

The various parametric combinations of streambed height, channel gradient, duration of the event, intensity, and skewness of the peak flows revealed interesting results. For example, in the cases of hydropeaking ($t_p/t_d = 0.5$) observed in dam operations or discharge from wastewater treatment plant (Casas-Mulet et al., 2015; Sawyer et al., 2009; Zhou et al., 2018), our results showed relatively higher discharge of older water and for a longer period of time when compared to lower t_p/t_d ratio. This was observed for all the bedform aspect ratios of streambed but only for lower slope values. The direct impact of hydropeaking, which may cause thermal peaking as well is observed in water chemistry and hence also hyporheic invertebrates as highlighted in the results by Bruno et al. (2009, 2013) and Jones (2014). Moreover, our results indicated that for the same event duration and peak flow intensity, HZs relatively release higher discharge of older water for bedforms like dunes and ripples when compared to alternating bars.

Using the framework of Damköhler number, we found that the HZ efficiency may increase during the peak flow event. Here the efficiency was seen as the potential for aerobic and anaerobic respiration hence was correlated to potential nitrification and denitrification in the streambed. During the peak flow events, the aerobic and anaerobic respiration increased (not with the same factor) with respect to the initial conditions. The formation of longest and deepest flow path was highly dependent on the local pressure gradient caused by the streambed topography, flow intensity and ambient groundwater flow. Zarnetske et al. (2011) showed that the denitrification in anaerobic zones of the HZ is limited by the supply of labile DOC. Additionally, the authors also suggested that only estimates of residence times and time scales for oxygen consumption are crucial to predict the locations of nitrification and denitrification (Zarnetske et al., 2012). Moreover, previous studies by Hinton et al. (1997) and Inamdar et al. (2004) have suggested higher and faster transport of DOC into deeper parts of HZ during an event hence acting as an electron donor when oxygen is depleted in the deeper parts of the streambed. Our results indicated potential development of larger areas of anoxic zones, that is, favorable for denitrification during the peak flow events. Assuming higher influx of labile DOC into the streambed during an event, the river-aquifer system can be highly efficient in removing nitrates postevent, especially for the bedforms like ripples and dunes. As the regions of anoxic zones are formed deeper into the

streambed during the event, transported labile DOC would help the denitrifying bacteria to complete the process of denitrification. These findings are similar to Trauth and Fleckenstein (2017) where there simulation results for an in-stream gravel bar showed higher rates of aerobic respiration and denitrification for higher peak flow intensities and longer durations of the event.

The mechanistic understanding of the dynamic hyporheic exchange presented in this manuscript is the preliminary step to predict the regional-scale water quality outcomes. The attenuation of nutrients and efficiency of transformation processes is moderated by the intensity of surface water exchange in the HZ as it determines the contact time of the water and solutes in the buffer zone (i.e., the HZ). As this exchange is highly dependent on the local conditions of the sites, the accurate quantification of HEF beginning from the small scale is essential to translate to the regional scale.

4.3. Limitations and Future Work

In our study, we have used a reduced-order numerical model of an idealized, uniform, and single type of bedform essentially to gain a deeper mechanistic understanding of the dynamic exchange processes occurring in HZs in result of peak flow events. While, for our systematic analyses, we considered a broad range of different scenario conditions (with regard to bedform topography, channel gradient, and peak flow event characteristics), there remain further variables and potentially impactful drivers that have not been analyzed in this study such as variability in streambed structural properties (Gomez-Velez et al., 2014) or the impacts of critical flows with the potential to mobilize the streambed materials (Simpson & Meixner, 2012; Wu et al., 2015). Combination of several bedform morphologies with topographic structure of the catchment determines the overall HEF (Caruso et al., 2016; Schmadel et al., 2017; Ward et al., 2018). This includes nested flow paths; however, in this manuscript we have only taken into consideration the shorter and local flow paths. Furthermore, we assumed only conditions without gaining or losing groundwater conditions. The analysis of potential additional impacts of net gains and losses of water and the resulting interference with peak flow event-driven hyporheic exchange remain as the focus of future investigations. Moreover, our simulations assume no temperature-induced effects with the impact of temporal fluctuations of water temperatures on resulting HEF (i.e., induced by diurnal surface water temperature oscillations). Considering earlier work on temperature effects on hyporheic exchange flow (Cardenas & Wilson, 2007), it appears promising to extend investigations toward potential temperature effects on HEF and temperature-dependent chemical reaction rates during transient flow conditions.

5. Conclusions

Interactions between bedform topography, channel gradient, and hydrodynamic forcings result in complex exchange of water and solute fluxes between the water column and underlying HZs. Our simulation results systematically explored the complex impacts of various peak flow events and geomorphic conditions on hyporheic exchange flow patterns and dynamics for a comprehensive range of scenarios for an idealized, uniform, and single type of bedform. Our results indicated dynamic expansion and contraction of the HZs during the event; however, in several cases this expansion was counteracted by strong ambient horizontal flow induced by larger slope values of the stream channel. Although the relative change (to baseflow conditions) in HEF (%) was unaffected by different values of channel slopes, absolute magnitudes varied substantially. The primary impact of peak flow events was observed on the residence time of the water in HZs. Intensification of discharge of younger and older water out of the SWI was evident at high intensities and longer durations of the event. Primarily, for streambed profiles with low slopes, events caused more discharge of older water for the higher bedform aspect ratios (i.e., for dunes and ripples). The direct influence of alterations in residence time distributions was observed in the efficiency of the HZs in developing larger areas of potential nitrification and denitrification.

Intricate understanding of processes such as denitrification is important to maintain water quality and aquatic life in the riverine systems. This is because denitrification process reduces nitrates from river-aquifer continuum, through a chain of intermediate reactions. However, incomplete denitrification in the streams result in the release of N_2O, an ozone-depleting substance into the atmosphere instead of molecular nitrogen (Briggs et al., 2015). Any dynamic alterations in river stage due to external hydrologic forcing can have substantial impact on streambed nutrient cycling and transformations. Such forcing can transport organic matter (and even contaminants) deep into the streambed, potentially increasing its contact time to favorable conditions required for transformations. As in the case of denitrification process, a peak flow event could lead to the transport of organic matter deeper into the alluvium where anoxic environments are present for the completion

of the process. This indicates that thorough investigation of river morphological and riparian characteristics and combination of peak flow event scenarios can be potentially adopted for managing and restoring river water chemistry.

Acknowledgments
This project is supported by Marie Curie ITN HypoTRAIN, which has received funding from European Union's Horizon 2020 research and innovation programme under Marie Skłodowska-Curie grant agreement 641939. Gomez-Velez is funded by the NSF grant EAR 1830172, the U.S. Geological Survey's River Corridor Powell Center, and the U.S. Department of Energy (DOE), Office of Biological and Environmental Research (BER), as part of BER's Subsurface Biogeochemistry Research Program (SBR). This contribution originates from the SBR Scientific Focus Area (SFA) at the Pacific Northwest National Laboratory (PNNL). We would also like to thank the Associate Editor and three anonymous reviewers for their insightful comments and feedback on the manuscript. All data required to reproduce the figures in this paper is available on the data repository of the University of Birmingham's library (https://edata.bham.ac.uk/).

References

Bear, J. (1972). *Dynamics of fluids in porous media*. New York: American Elsevier.
Boano, F., Camporeale, C., Revelli, R., & Ridolfi, L. (2006). Sinuosity-driven hyporheic exchange in meandering rivers. *Geophysical Research Letters*, *33*, L18406. https://doi.org/10.1029/2006GL027630
Boano, F., Harvey, J. W., Marion, A., Packman, A. I., Revelli, R., Ridolfi, L., & Wörman, A. (2014). Hyporheic flow and transport processes: Mechanisms, models, and biogeochemical implications: Hyporheic flow and transport proceses. *Reviews of Geophysics*, *52*, 603–679. https://doi.org/10.1002/2012RG000417
Boano, F., Revelli, R., & Ridolfi, L. (2007). Bedform-induced hyporheic exchange with unsteady flows. *Advances in Water Resources*, *30*(1), 148–156.
Boano, F., Revelli, R., & Ridolfi, L. (2013). Modeling hyporheic exchange with unsteady stream discharge and bedform dynamics. *Water Resources Research*, *49*, 4089–4099. https://doi.org/10.1002./wrcr.20322
Boulton, A. J., Findlay, S., Marmonier, P., Stanley, E. H., & Valett, H. M. (1998). The functional significance of the hyporheic zone in streams and rivers. *Annual Review of Ecology and Systematics*, *29*(1), 59–81.
Bridge, J. S. (2009). *Rivers and floodplains: Forms, processes, and sedimentary record*. John Wiley & Sons.
Briggs, M. A., Day-Lewis, F. D., Zarnetske, J. P., & Harvey, J. W. (2015). A physical explanation for the development of redox microzones in hyporheic flow. *Geophysical Research Letters*, *42*, 4402–4410. https://doi.org/10.1002/2015GLO64200
Brunke, M., & Gonser, T. (1997). The ecological significance of exchange processes between rivers and groundwater. *Freshwater biology*, *37*(1), 1–33.
Bruno, M. C., Maiolini, B., Carolli, M., & Silveri, L. (2009). Impact of hydropeaking on hyporheic invertebrates in an Alpine Stream (Trentino, Italy). In *Annales De Limnologie-International Journal of Limnology* (Vol. 45, No. 3, pp. 157–170). EDP Sciences.
Bruno, M. C., Siviglia, A., Carolli, M., & Maiolini, B. (2013). Multiple drift responses of benthic invertebrates to interacting hydropeaking and thermopeaking waves. *Ecohydrology*, *6*(4), 511–522.
Buffington, J., & Tonina, D. (2009). Hyporheic exchange in mountain rivers II: Effects of channel morphology on mechanics, scales, and .... interscience.wiley.com.
Cardenas, M. B. (2015). Hyporheic zone hydrologic science: A historical account of its emergence and a prospectus. *Water Resources Research*, *51*, 3601–3616. https://doi.org/10.1002/2015WR017028
Cardenas, M. B., & Wilson, J. (2006). The influence of ambient groundwater discharge on exchange zones induced by current–bedform interactions. *Journal of Hydrology*, *331*(1), 103–109.
Cardenas, M. B., & Wilson, J. L. (2007). Effects of current–bed form induced fluid flow on the thermal regime of sediments. *Water Resources Research*, *43*, W08431. https://doi.org/10.1029/2006WR005343
Cardenas, M. B., Wilson, J., & Zlotnik, V. A. (2004). Impact of heterogeneity, bed forms, and stream curvature on subchannel hyporheic exchange. *Water Resources Research*, *40*, W08307. https://doi.org/10.1029/2004WR003008
Caruso, A., Ridolfi, L., & Boano, F. (2016). Impact of watershed topography on hyporheic exchange. *Advances in Water Resources*, *94*, 400–411.
Casas-Mulet, R., Alfredsen, K., Hamududu, B., & Timalsina, N. P. (2015). The effects of hydropeaking on hyporheic interactions based on field experiments. *Hydrological processes*, *29*(6), 1370–1384.
Cooper, H. H., & Rorabaugh, M. I. (1963). *Groundwater movements and bank storage due to flood stages in surface streams* (U.S. Geological Survey Water Supply Pap. 1536-J). Washington, DC: United State Printing Office.
Dingman, S. L. (2009). *Fluvial hydraulics*. Oxford; New York: Oxford University Press.
Dudley-Southern, M., & Binley, A. (2015). Temporal responses of groundwater-surface water exchange to successive storm events. *Water Resources Research*, *51*, 1112–1126.
Elliott, A. H., & Brooks, N. H. (1997). Transfer of nonsorbing solutes to a streambed with bed forms: Theory. *Water Resources Research*, *33*(1), 123–136.
Fritz, B. G., & Arntzen, E. V. (2007). Effect of rapidly changing river stage on uranium flux through the hyporheic zone. *Ground Water*, *45*(6), 753–760.
Gomez, J., & Wilson, J. (2013). Age distributions and dynamically changing hydrologic systems: Exploring topography-driven flow. *Water Resources Research*, *49*, 1503–1522.
Gomez, J. D., Wilson, J. L., & Cardenas, M. B. (2012). Residence time distributions in sinuosity-driven hyporheic zones and their biogeochemical effects. *Water Resources Research*, *48*, W09533. https://doi.org/10.1002/wrcr.20127
Gomez-Velez, J. D., & Harvey, J. W. (2014). A hydrogeomorphic river network model predicts where and why hyporheic exchange is important in large basins. *Geophysical Research Letters*, *41*, 6403–6412. https://doi.org/10.1002/2014GL061099
Gomez-Velez, J. D., Harvey, J. W., Cardenas, M. B., & Kiel, B. (2015). Denitrification in the Mississippi River network controlled by flow through river bedforms. *Nature Geoscience*, *8*, 941–945. https://doi.org/10.1038/ngeo2567
Gomez-Velez, J. D., Krause, S., & Wilson, J. L. (2014). Effect of low-permeability layers on spatial patterns of hyporheic exchange and groundwater upwelling. *Water Resources Research*, *50*, 5196–5215. https://doi.org/10.1002/2013WR015054
Gomez-Velez, J. D., Wilson, J. L., Cardenas, M. B., & Harvey, J. W. (2017). Flow and residence times of dynamic river bank storage and sinuosity-driven hyporheic exchange. *Water Resources Research*, *53*, 8572–8595. https://doi.org/10.1002/2017wr021362
Gooseff, M. N. (2010). Defining hyporheic zones–advancing our conceptual and operational definitions of where stream water and groundwater meet. *Geography Compass*, *4*(8), 945–955.
Gu, C., Hornberger, G. M., Herman, J. S., & Mills, A. L. (2008). Effect of freshets on the flux of groundwater nitrate through streambed sediments. *Water resources research*, *44*, W05415. https://doi.org/10.1029/2007WR006488
Hannah, D. M., Malcolm, I. A., & Bradley, C. (2009). Seasonal hyporheic temperature dynamics over riffle bedforms. *Hydrological Processes*, *23*(15), 2178–2194. https://doi.org/ 10.1002/hyp.7256
Harvey, J. W., Böhlke, J. K., Voytek, M. A., Scott, D., & Tobias, C. R. (2013). Hyporheic zone denitrification: Controls on effective reaction depth and contribution to whole-stream mass balance. *Water Resources Research*, *49*, 6298–6316. https://doi.org/10.1002/wrcr.20492
Harvey, J., & Gooseff, M. (2015). River corridor science: Hydrologic exchange and ecological consequences from bedforms to basins. *Water Resources Research*, *51*, 6893–6922. https://doi.org/10.1002/2015WR017617

Hinton, M., Schiff, S., & English, M. (1997). The significance of storms for the concentration and export of dissolved organic carbon from two Precambrian Shield catchments. *Biogeochemistry*, *36*(1), 67–88.
Inamdar, S. P., Christopher, S. F., & Mitchell, M. J. (2004). Export mechanisms for dissolved organic carbon and nitrate during summer storm events in a glaciated forested catchment in New York, USA. *Hydrological Processes*, *18*(14), 2651–2661.
Jones, N. (2014). The dual nature of hydropeaking rivers: Is ecopeaking possible? *River Research and Applications*, *30*(4), 521–526.
Kaufman, M. H., Cardenas, M. B., Buttles, J., Kessler, A. J., & Cook, P. L. (2017). Hyporheic hot moments: Dissolved oxygen dynamics in the hyporheic zone in response to surface flow perturbations. *Water Resources Research*, *53*, 6642–6662. https://doi.org/10.1002/2016WR020296
Krause, S., Hannah, D. M., & Blume, T. (2011). Interstitial pore-water temperature dynamics across a pool-riffle-pool sequence. *Ecohydrology*, *4*(4), 549–563.
Krause, S., Hannah, D., Fleckenstein, J., Heppell, C., Kaeser, D., Pickup, R., et al. (2011). Inter-disciplinary perspectives on processes in the hyporheic zone. *Ecohydrology*, *4*(4), 481–499.
Krause, S., Tecklenburg, C., Munz, M., & Naden, E. (2013). Streambed nitrogen cycling beyond the hyporheic zone: Flow controls on horizontal patterns and depth distribution of nitrate and dissolved oxygen in the upwelling groundwater of a lowland river. *Journal of Geophysical Research: Biogeosciences*, *118*, 54–67. https://doi.org/ 10.1029/2012JG002122
Malcolm, I., Soulsby, C., Youngson, A., Hannah, D., McLaren, I., & Thorne, A. (2004). Hydrological influences on hyporheic water quality: Implications for salmon egg survival. *Hydrological Processes*, *18*(9), 1543–1560.
Malzone, J. M., Anseeuw, S. K., Lowry, C. S., & Allen-King, R. (2016). Temporal hyporheic zone response to water table fluctuations. *Groundwater*, *54*(2), 274–285. https://doi.org/ 10.1111/gwat.12352
Malzone, J. M., Lowry, C. S., & Ward, A. S. (2016). Response of the hyporheic zone to transient groundwater fluctuations on the annual and storm event time scales. *Water Resources Research*, *52*, 5301–5321. https://doi.org/ 10.1002/2015WR018056
McCallum, J. L., & Shanafield, M. (2016). Residence times of stream-groundwater exchanges due to transient stream stage fluctuations. *Water Resources Research*, *52*, 2059–2073. https://doi.org/10.1002/2015WR017441
Millington, R., & Quirk, J. (1961). Permeability of porous solids. *Transactions of the Faraday Society*, *57*, 1200–1207.
O'Connor, B. L., & Harvey, J. W. (2008). Scaling hyporheic exchange and its influence on biogeochemical reactions in aquatic ecosystems. *Water Resources Research*, *44*, W12423. https://doi.org/10.1029/2008WR007160
Ocampo, C. J., Oldham, C. E., & Sivapalan, M. (2006). Nitrate attenuation in agricultural catchments: Shifting balances between transport and reaction. *Water Resources Research*, *42*, W01408. https://doi.org/10.1029/2004WR003773
Packman, A., Salehin, M., & Zaramella, M. (2004). Hyporheic exchange with gravel beds: Basic hydrodynamic interactions and bedform-induced advective flows. *Journal of Hydraulic Engineering*, *130*, 647.
Pinay, G., Peiffer, S., De Dreuzy, J.-R., Krause, S., Hannah, D. M., Fleckenstein, J. H., et al. (2015). Upscaling nitrogen removal capacity from local hotspots to low stream orders' drainage basins. *Ecosystems*, *18*(6), 1101–1120.
Ryan, R. J., & Boufadel, M. C. (2006). Influence of streambed hydraulic conductivity on solute exchange with the hyporheic zone. *Environmental Geology*, *51*(2), 203–210.
Sanz-Prat, A., Lu, C., Amos, R. T., Finkel, M., Blowes, D. W., & Cirpka, O. A. (2016). Exposure-time based modeling of nonlinear reactive transport in porous media subject to physical and geochemical heterogeneity. *Journal of Contaminant Hydrology*, *192*, 35–49.
Sanz-Prat, A., Lu, C., Finkel, M., & Cirpka, O. A. (2015). On the validity of travel-time based nonlinear bioreactive transport models in steady-state flow. *Journal of Contaminant Hydrology*, *175*, 26–43.
Sawyer, A. H., Cardenas, M. B., Bomar, A., & Mackey, M. (2009). Impact of dam operations on hyporheic exchange in the riparian zone of a regulated river. *Hydrological Processes*, *23*(15), 2129–2137.
Schmadel, N. M., Ward, A. S., Lowry, C. S., & Malzone, J. M. (2016). Hyporheic exchange controlled by dynamic hydrologic boundary conditions. *Geophysical Research Letters*, *43*, 4408–4417. https://doi.org/ 10.1002/2016GL068286
Schmadel, N. M., Ward, A. S., & Wondzell, S. M. (2017). Hydrologic controls on hyporheic exchange in a headwater mountain stream. *Water Resources Research*, *53*, 6260–6278. https://doi.org/10.1002/2017wr020576
Simpson, S. C., & Meixner, T. (2012). Modeling effects of floods on streambed hydraulic conductivity and groundwater-surface water interactions. *Water Resources Research*, *48*, W02515. https://doi.org/10.1029/2011WR011022
Stonedahl, S. H., Harvey, J. W., Wörman, A., Salehin, M., & Packman, A. I. (2010). A multiscale model for integrating hyporheic exchange from ripples to meanders. *Water Resources Research*, *46*, W12539. https://doi.org/10.1029/2009WR008865
Tonina, D., & Buffington, J. (2009a). Hyporheic exchange in mountain rivers I: Mechanics and environmental effects. *Geography Compass*, *3*(3), 1063–1086.
Tonina, D., & Buffington, J. (2009b). Hyporheic exchange in mountain rivers I: Mechanics and environmental effects. *Geography Compass*, *3*(3), 1063–1086.
Tonina, D., & Buffington, J. M. (2011). Effects of stream discharge, alluvial depth and bar amplitude on hyporheic flow in pool-riffle channels. *Water Resources Research*, *47*, W08508. https://doi.org/10.1029/2010WR009140
Trauth, N., & Fleckenstein, J. H. (2017). Single discharge events increase reactive efficiency of the hyporheic zone. *Water Resources Research*, *53*, 779–798. https://doi.org/10.1002/2016WR019488
Triska, F. J., Kennedy, V. C., Avanzino, R. J., Zellweger, G. W., & Bencala, K. E. (1989). Retention and transport of nutrients in a third-order stream in northwestern California: Hyporheic processes. *Ecology*, *70*, 1893–1905.
Ward, A. S., Gooseff, M. N., Voltz, T. J., Fitzgerald, M., Singha, K., & Zarnetske, J. P. (2013). How does rapidly changing discharge during storm events affect transient storage and channel water balance in a headwater mountain stream? *Water Resources Research*, *49*, 5473–5486. https://doi.org/10.1002/wrcr.20434
Ward, A. S., Schmadel, N. M., & Wondzell, S. M. (2018). Time-variable transit time distributions in the hyporheic zone of a headwater mountain stream. *Water Resources Research*, *54*, 2017–2036. https://doi.org/10.1002/2017WR021502
Ward, A. S., Schmadel, N. M., Wondzell, S. M., Gooseff, M. N., & Singha, K. (2017). Dynamic hyporheic and riparian flow path geometry through base flow recession in two headwater mountain stream corridors. *Water Resources Research*, *53*, 3988–4003. https://doi.org/ 10.1002/2016WR019875
Wondzell, S. M., & Swanson, F. J. (1999). Floods, channel change, and the hyporheic zone. *Water Resources Research*, *35*(2), 555–567.
Wörman, A., Packman, A. I., Marklund, L., Harvey, J. W., & Stone, S. H. (2006). Exact three-dimensional spectral solution to surface-groundwater interactions with arbitrary surface topography. *Geophysical Research Letters*, *33*, L07402. https://doi.org/10.1029/ 2006GL025747
Wu, G., Shu, L., Lu, C., Chen, X., Zhang, X., Appiah-Adjei, E. K., & Zhu, J. (2015). Variations of streambed vertical hydraulic conductivity before and after a flood season. *Hydrogeology Journal*, *23*(7), 1603–1615.

Zarnetske, J. P., Haggerty, R., Wondzell, S. M., & Baker, M. A. (2011). Dynamics of nitrate production and removal as a function of residence time in the hyporheic zone. *Journal of Geophysical Research*, *116*, G01025. https://doi.org/10.1029/2010JG001356

Zarnetske, J. P., Haggerty, R., Wondzell, S. M., Bokil, V. A., & González-Pinzón, R. (2012). Coupled transport and reaction kinetics control the nitrate source-sink function of hyporheic zones. *Water Resources Research*, *48*, W11508. https://doi.org/10.1029/2012WR011894

Zhou, T., Bao, J., Huang, M., Hou, Z., Arntzen, E., Song, X., et al. (2018). Riverbed hydrologic exchange dynamics in a large regulated river reach. *Water Resources Research*, *54*, 2715–2730. https://doi.org/10.1002/2017WR020508